

Studies on Corrosion Resistance and Electrochemical Behavior of Pb-Sb-As-S Alloys as Positive Grids in Lead-acid Batteries

Z. Ghasemi and A. Tizpar*

R&D of Niru Battery Manufacturing CO., Pasdaran, P.O. Box 19575-361, Tehran, Iran

*E-mail: atizpar@yahoo.com

Received: 1 June 2007 / Accepted: 6 August 2007 / Published: 1 September 2007

The effects of sulfur addition in the range of 0.003-0.01wt.% on the corrosion resistance, electrochemical properties and gas evolution of Pb-Sb-As-S alloy in sulfuric acid solution were investigated by Linear sweep voltammetry, cyclic voltammetry, weight loss measurements, electrochemical impedance spectroscopy, chronoamperometry and scanning electron microscopy at room temperature. Sulfur added to lead alloy shifts the corrosion potential to negative values. Both oxygen and hydrogen evolution overpotentials were found to be higher for the alloys containing sulfur respect to samples without sulfur. The structures of low-antimony-arsenic alloy surfaces doped by sulfur were studied by using SEM. The experimental results show that, sulfur added to Pb-Sb-As alloy inhibits the growth of the anodic β -PbO₂ film and increases the reaction resistance. Impedance spectroscopy measurements showed that the sulfur addition decreased the conductivity of β -PbO₂ film on the lead alloy. In addition, the effect of sulfur on the hardness of the positive grids and batteries discharge capacities made of these grids was studied.

Keywords: corrosion; sulfur; lead-acid battery; grid alloy; surface

1. INTRODUCTION

Lead-antimony alloys are known for preparing grids in lead-acid electric accumulators. Pure lead is too weak and antimony is added to improve the strength and castability of the alloy. However, at concentrations of above 4% there is a significant tendency for the antimony to be released from the grid into the electrolyte during service and on charging to be deposited on the spongy lead of the negative plate. These results in a reduction of the hydrogen overpotential and the local cells of lead and antimony set up on the negative plate also cause loss of charge on open circuit. It is desirable to reduce

the antimony content to as low as possible to reduce open circuit losses and to render the battery resistant to the bad effects of overcharging such as tend to occur with automotive batteries charged from alternating current sources, e.g. alternators. Lead-antimony alloys having a lower than conventional antimony content provide the desired strength, but in practice grids containing for instance 1.5-3.5wt% antimony do not function well in lead-acid batteries because of their tendency for cracking and their brittleness. This is apparently caused by coarse dendritic [1,2]. The reduction of antimony content leads to deterioration in the mechanical properties and in the castability of the alloys. This can be partly compensated by the introduction the small amounts of the other elements such as arsenic, sulfur and selenium [3-5]. Arsenic exerts two major effects on the properties of lead-antimony alloys (i) it increases the rate of age-hardening which in practical terms, means decreasing the time that a grid has to be stored after casting before further processing; (ii) it increases the creep resistance which in turn, increases the durability of the positive plate, especially during deep cycling [3]. We used the alloy composition of Pb- Sb- As- S. These alloys are currently used in the manufacture of positive grids at Niru Battery manufacturing company for batteries.

1.1 Effect of minor elements on alloy properties

The basic requirements for lead alloys are: good mechanical characteristics, i.e., adequate hardness and strength and little mechanical and heat distortion; good corrosion resistance, i.e., light intercrystalline corrosion and low corrosion rate; good casting characteristics; good weldability; little pollution and low cost. To satisfy these requirements, various alloys have been studied. Today, only three types of alloys are widely used, namely:

- high antimony alloy, 4-11 wt.% Sb, with traces of arsenic, tin, selenium, etc.;
- low antimony alloy, 0.8-3 wt.% Sb, with some arsenic, tin, selenium, copper, sulfur, etc.;
- Pb-Ca- Sn-Al multi-element alloy [6].

To increase the corrosion resistance, some additives can be used [7, 8]. One of these additives is silver. Silver has been added to lead alloys for grid and post alloys in lead-acid batteries for many years. In the past 10 years, the positive grids of SLI batteries have used the addition of 125-500 ppm silver to lead-calcium-tin alloy positive grids to reduce corrosion particularly at elevated temperatures. The benefits have been described by prengaman [9,10] and Rao et al. [11,12]. Also, there are some literature data for the application of sulfur as an alloying additive to lead alloys [4,13], but the influence of sulfur on electrochemical behavior, corrosion resistance and gas evolution reaction rate of Pb-Sb-As alloys has been scarcely studied. The purpose of this paper is to investigate the effect of sulfur introduced as an alloying additive on the corrosion resistance, electrochemical behavior and H₂&O₂ evolution of Pb-Sb-As alloys as positive grids in the lead-acid batteries. Also, we investigated the effect of sulfur on the hardness of the positive grids and batteries discharge capacities made of these grids.

2. EXPERIMENTAL

2.1. Weight-loss measurements

A nominal alloy composition (Pb-1.8wt.%Sb-0.1wt.%As) was used as the base alloy. Sulfur (99.99%) in the range of 0.003-0.01wt.% was added to the molten alloy at about 700 °C, then the melt was poured in the cast iron mould and cast rods with surface area of 8 cm² were removed from the moulds at about 140 °C. The exact percentages of sulfur in the alloys were determined by atomic absorption spectrophotometer (Analyst 800). Before every experiment the rods were washed, degreased with acetone, rinsed with double-distilled water, dried, weighted and introduced in 1.28 sp.gr. H₂SO₄ solution. The rods were polarized with current density of 10 mAcm⁻² galvanostatically for 24h. Then they were taken out from the solution. All corrosion products were removed with hot alkaline saccharose solution. Then the rods rinsed with water, dried and weighted. Four rods were used for every alloy composition and a new test piece was used for every experiment.

2.2. Electrochemical measurements

Linear sweep voltammetry (LSV), cyclic voltammetry (CV), chronoamperometry (CA) and electrochemical impedance spectroscopy (EIS) were carried out by using a Galvanostat/Potentiostat Autolab (PCSTAT 20) apparatus connected to a PIV PC computer. Lead alloy rods with composition of those mentioned in the previous section were used for LSV test. The rod alloys were used as working electrodes. These were mounted so that a cross-sectional surface area of 0.08cm² was exposed in the electrolyte. A flat working electrode surface was obtained by mechanical polishing with emery papers 240, 800, 1500 and 2500. The working electrodes were degreased with acetone and washed with double-distilled water before immersing in the electrolyte. Before every experiment a cathodic polarization at a potential of -1.6V was performed for 10 min in order to remove any oxidation products formed by aerial oxidation during pretreatments. All investigations were performed in 1.28 sp.gr. H₂SO₄ solution and a three-compartment cell were used in the experiments. A platinum plate served as a counter electrode and an Hg/Hg₂SO₄ electrode was used as the reference electrode. All potentials are referred to this scale. Each polarization was run three times and corrosion potentials and currents were reproducible within ±5mV and ±1μA, respectively.

CV method was carried out to investigate the Pb-Sb-As base alloy electrochemical behavior, determine potential region of β-PbO₂ and to characterize the gas evolution reactions that take place on the lead alloy, by using potentiostat and electrolyte described in the above paragraph. Cyclic voltammograms were recorded at a scan rate of 20mVs⁻¹ in the PbO₂/PbSO₄ couple potential region of (0.5–1.5V vs. Hg/Hg₂SO₄) and oxygen and hydrogen evolution potential regions.

CA method was used to study the formation of β-PbO₂ by means of potentiostatic transients. The lead electrode has been initially maintained at a potential of -1.6 V (vs. Hg/Hg₂SO₄electrode) for 10 min to remove any oxidation products, then potential was stepped to 1.45V to produce β-PbO₂ film.

Impedance measurements were carried out in a frequency of 100 kHz to 1 mHz with amplitude of 10mV peak-to-peak using ac signals. Electrochemical impedance measurements were performed by

using the lead alloys as working electrodes coated with thin layer of β -PbO₂ that were prepared via application a constant potential of 1.45V for 60 min. GPES and FRA (v. 4.9) soft wares were used to analyze the data.

2.3. Discharge capacity of cells

At first the grids with identified compositions of sulfur were casted by a 6SB₃ motorcycle's mould. Positive paste were prepared by mixing lead oxide supplied by Niru Battery Mfg CO., with water, sulfuric acid, according to conventional formulation in the manufacture of motorcycle MF battery. The paste was then manually applied onto the grids with a plastic scraper. The pasted plates were cured at 60 °C with a relative humidity over 90% for 48 h in a curing set (VC 4018 m. ultra - Vit). The used cell for this test consists of one positive plate (with various compositions of sulfur) and two negative plates (that pasted, cured and charged previously) of a 6SB₃ motorcycle MF battery. The electrolyte is sulfuric acid with specific gravity of 1.28. The discharge capacity variations of the 2V cells were assessed by employing a solartron 1470, a multi- channel battery tester system. An initial formation algorithm was performed in 1.05 sp.gr. H₂SO₄ solution. This procedure consists of: 1-Rest for 0.5 h, 2-Constant 10mA/g for 3.33 h, 3- Constant 20mA/g for 5 h, 4- Constant 30mA/g for 4.45 h, 5- Rest for 0.5 h, 6- Constant 33.33mA/g for 1 h, 7- Rest for 0.5 h, 8- Constant 6.66mA/g for 1 h, 9- Rest for 10min

The formation was completed with repeating the steps for two times. The cells were discharged at -1A until the voltage had fallen to 1.5 V and charged at 0.9 A until the voltage had risen to 2.6 V. The electrolyte was 1.28 sp.gr. H₂SO₄ solution and the charge/discharge procedure was repeated until the discharge capacity had fallen bellow 10% of initial value.

2.4. Scanning electron microscopy

The surface morphology was observed by using a SEM apparatus (Philips XL 30). The cross-sections of mounted rod alloys with different concentrations of sulfur were polished mechanically with emery papers 800, 1500 and 2500. All samples were degreased with acetone and washed with distilled water. Finally their polished surfaces were examined with scanning electron microscopy to understand the distribution quality of sulfur in the alloy structure.

3. RESULTS AND DISCUSSION

3.1. Weight-loss measurements

Weight variation of lead alloy rods (with 8 cm² surface area) in 1.28 sp.gr. H₂SO₄ solution in the absence and presence of sulfur as an alloying additive were determined after 24h galvanostatically polarization with current density of 10 mAcm⁻². The corrosion rates of the alloys were compared in terms of the weight-losses. Fig. 1 shows the weight-losses versus different sulfur concentrations in the alloy.

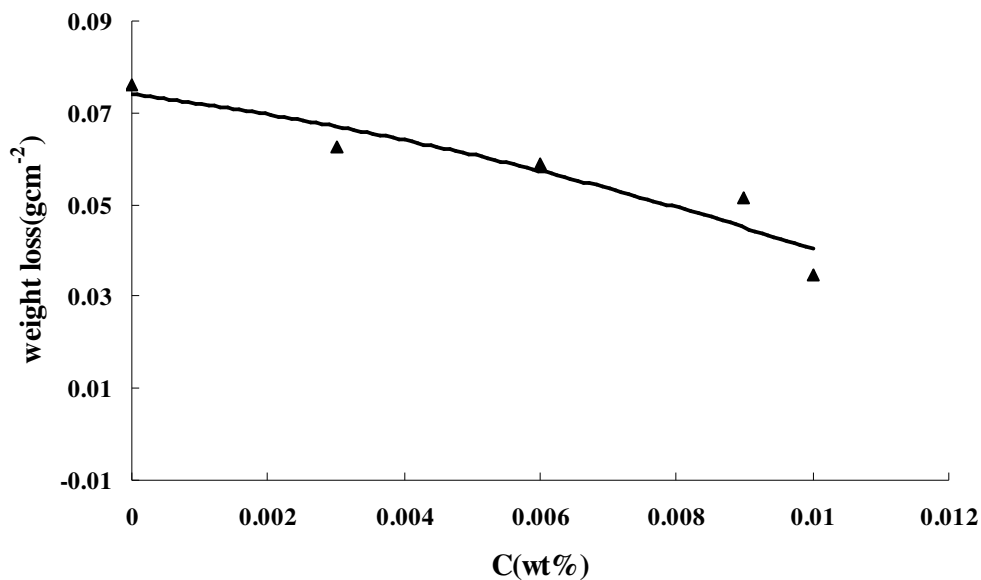


Figure 1. Weight loss vs. concentration curves for Pb-Sb-As-S alloys

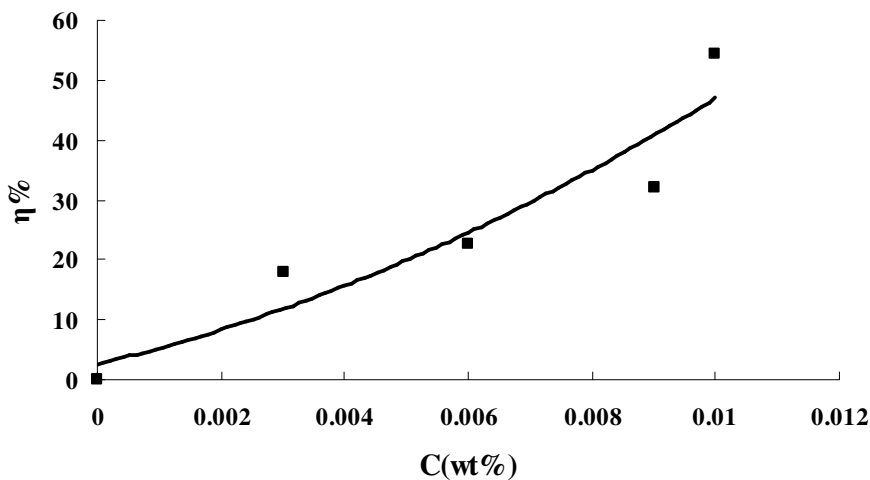


Figure 2. Inhibition efficiencies of different concentrations of sulfur in 1.28 sp.gr. H₂SO₄ solution

It can be seen that with increasing sulfur concentration in the alloy, the inhibition efficiencies increase. In fact, the alloys without sulfur corrode more easily than those with certain sulfur concentrations. The inhibition efficiencies of sulfur are calculated according to:

$$\eta (\%) = \frac{W_{\text{free}} - W_{\text{add}}}{W_{\text{free}}} \times 100$$

where W_{free} and W_{add} are the weight-losses of the lead alloys due to the dissolution in 1.28 sp.gr H_2SO_4 solution in the absence and presence of the different concentrations of sulfur in the alloys, respectively.

The inhibition efficiencies of different concentrations of sulfur are given in Fig.2. It can be seen that, the weight –loss of lead alloy depends on concentration of sulfur.

3.2. LSV

Tafel plot is often used to describe the rate of the electrochemical reaction at the cathodic potential [14], which can be shown as follow:

$$\eta = a + b \log i, b = \frac{2.3RT}{anF} \tag{1}$$

where a and b are constants. Assuming $\frac{d\eta}{di} = b \frac{1}{2.3i} = R_p$, Eq. (1) can be written as:

$$i = \frac{2.3RT}{anF} \cdot \frac{1}{R_p} \tag{2}$$

Substituting the Eq. (2) into Eq. (1), Eq. (3) is obtained:

$$\begin{aligned} \eta &= -b \log i_0 + b \log \frac{2.3RT}{anF} + b \log \frac{1}{R_p} \\ &= a + b \log \frac{2.3RT}{anF} + b \log \frac{1}{R_p} \end{aligned} \tag{3}$$

where $a = -b \log i_0$ and i_0 is the exchange current density. From Eq. (3), it can be found that there is a linear relationship between η and $\log \frac{1}{R_p}$, and b is the slope. Fig.3 shows the effect of sulfur concentration on polarization curves of lead alloy corrosion.

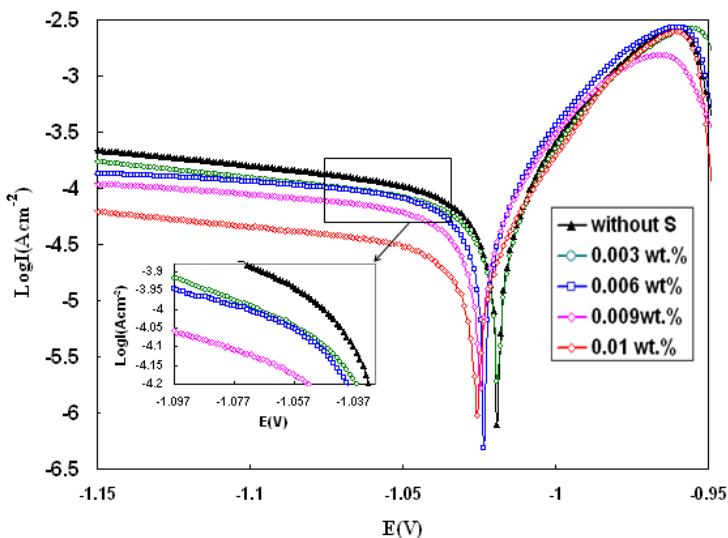


Figure 3. Polarization curves of the sulfur effect on Pb-Sb-As-S alloys in 1.28 sp.gr. H_2SO_4 solution

The potentials were swept from -1.15 to -0.85V versus Hg/Hg₂SO₄ reference electrode with sweep rate of 5mVs⁻¹. We fitted the values by extrapolation of the anodic and cathodic regions on the curves. The fitted values can depend strongly on the limits of the curves chosen for the fit, and these limits must be chosen carefully.

Table1. Corrosion data for Pb-Sb-As-S alloys with different concentrations of sulfur obtained from linear polarization method

Sample (wt. %)	$I_{\text{corr}}(\text{Acm}^{-2})$	$R_p(\Omega)$	Corr.Rate(mm/year)
Without S	$17.045 \cdot 10^{-4}$	$10.045 \cdot 10^2$	50.743
0.003	$13.888 \cdot 10^{-4}$	$11.977 \cdot 10^2$	41.468
0.006	$13.307 \cdot 10^{-4}$	$12.873 \cdot 10^2$	39.564
0.009	$11.634 \cdot 10^{-4}$	$14.651 \cdot 10^2$	34.706
0.01	$66.248 \cdot 10^{-5}$	$25.158 \cdot 10^2$	20.559

Corrosion parameters in the absence and presence of sulfur obtained from curves are given in Table 1. Generally with increasing sulfur concentration, the corrosion current density and corrosion rate decrease and polarization resistance increases. With increasing sulfur concentration, E_{corr} shifts to negative values (Fig. 4).

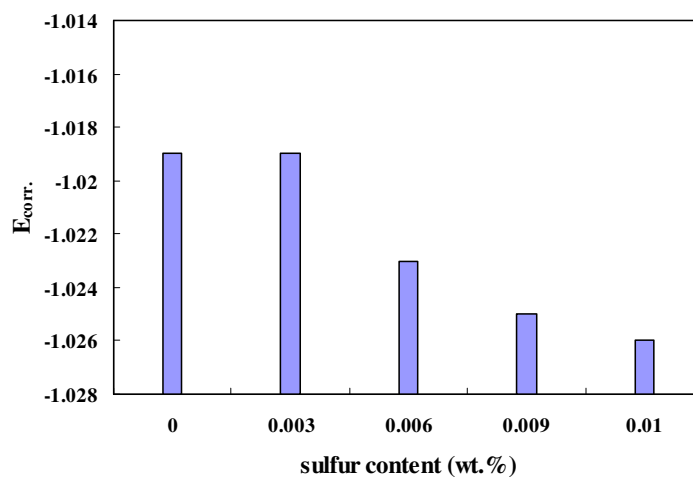


Figure 4. E_{corr} vs. concentration variations for Pb-Sb-As-S alloys in LSV method

The anodic corrosion current density i_{corr} will be lower on the electrodes with sulfur addition than on electrodes without sulfur. Therefore high corrosion resistance alloys can be obtained with sulfur additions.

3.3. SEM

Fig. (5 a,b) shows the phase diagrams of dilute Pb-S alloys [15]. As can be seen, sulfur can not insert into the lead lattice and replace any atoms of lead. The electronegativity of sulfur is quite different from that of lead and a compound is formed between the two elements with a composition of PbS. During cooling, this compound precipitates in the molten alloy in a finely-divided form and acts as nuclei for crystallizing lead-antimony-arsenic grains to give a fine-grain alloy and better castability. Casting of such alloys requires higher temperatures that must be rigidly maintained in order to avoid losses of nucleating agents via deposition in the molten metal before casting of the grids has been completed. Sulfur is added to the alloy as a grain refiner, due to the formation of lead sulfide nuclei at the inception of solidification. In the absence of such nuclei, freezing of the alloy will first occur on the cool walls of the mould, thus a columnar structure is obtained. Columnar structure is not desired because it leads to a poor castability due to a poor metal flow to those portions of the casting mould last to freeze and to non-uniform distribution of antimony, which contributes to increased gassing rates.

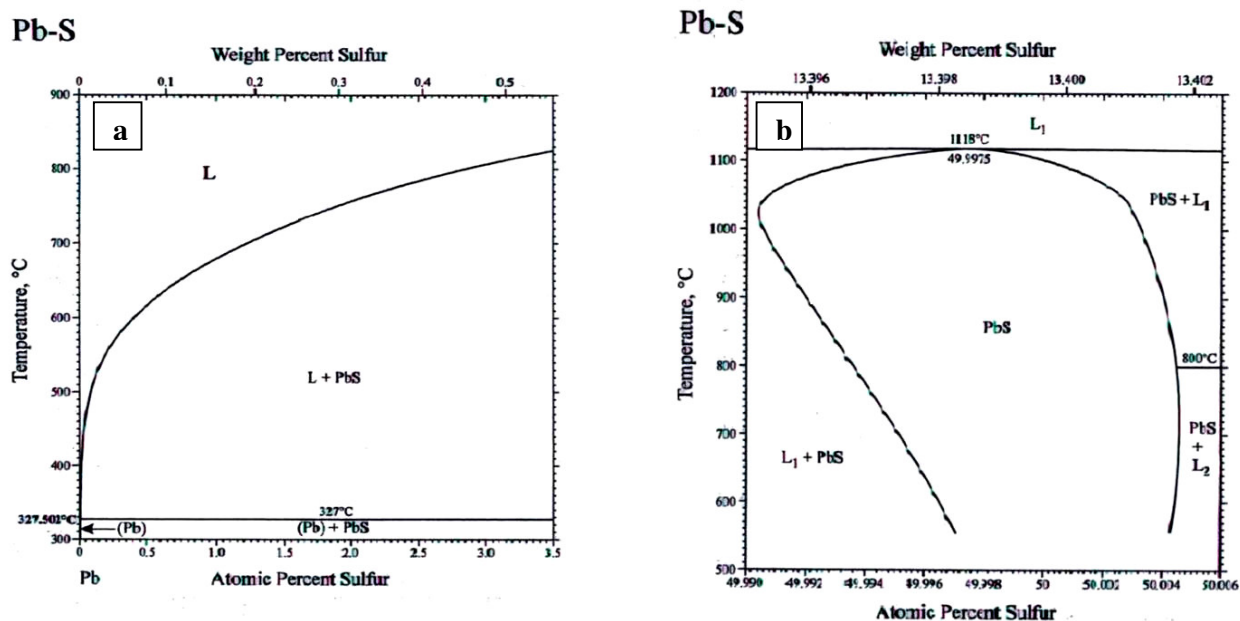
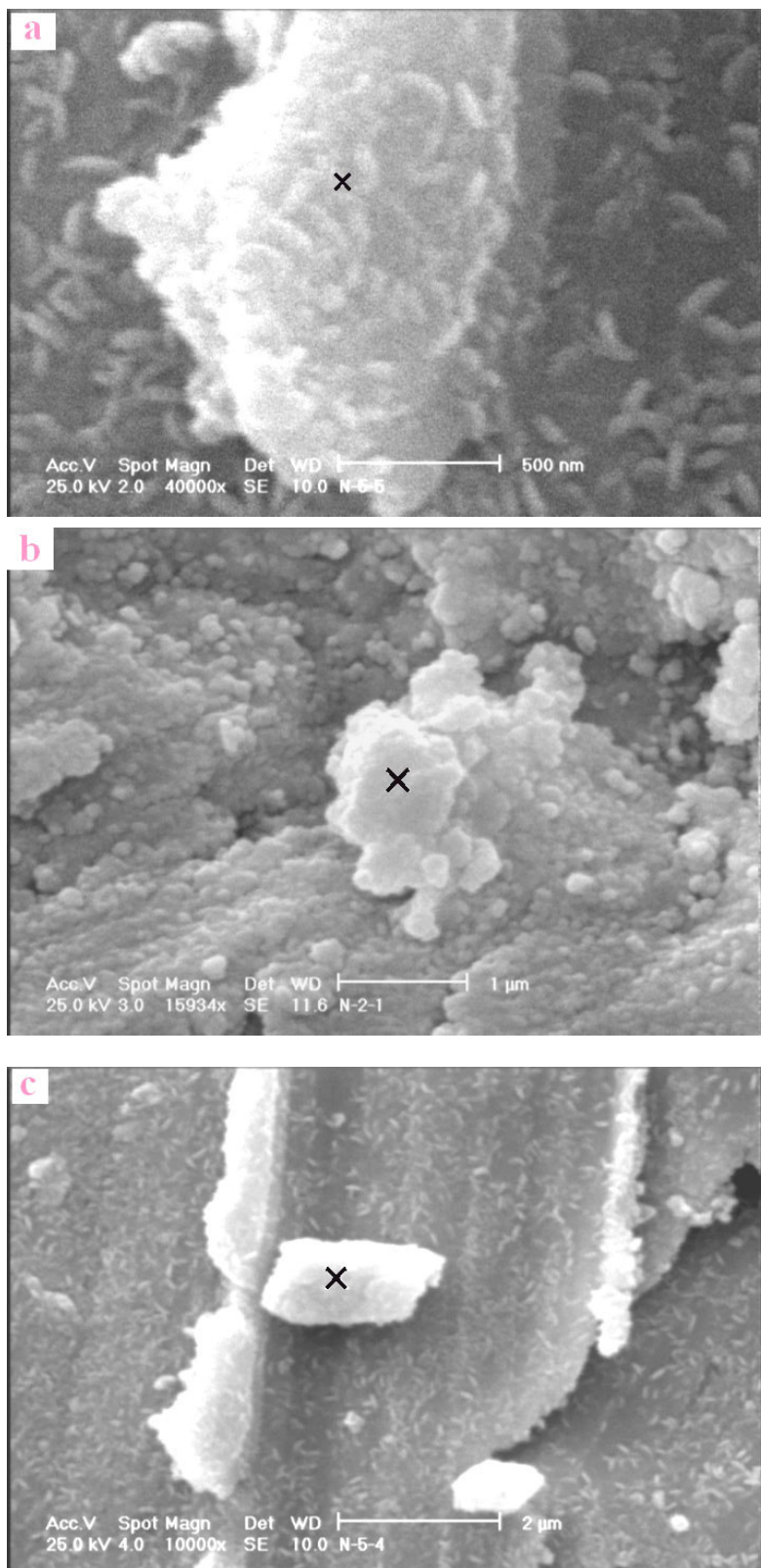


Figure 5. Phase diagrams of dilute PbS alloys

Proper selection of the grain refiner materials and the amount of them is very important since formation of the nucleating particles too early or too late in the solidification process, makes them ineffective. At low antimony levels in the lead alloy of this investigation, and for manufacturing thin grids, the sulfur concentration assumes greater importance. Hot cracking of the alloy is a result of poor castability and columnar structure. In general, a sufficient amount of sulfur is added to the alloy to

achieve good casting and avoid hot cracking of the alloy. The structures of lead-antimony-arsenic alloy surfaces doped by sulfur are shown in Fig. 6 and 7. Fig. 6 shows the SEM images of cross-sectional surface area of Pb-Sb-As-S alloys with different concentrations of sulfur.



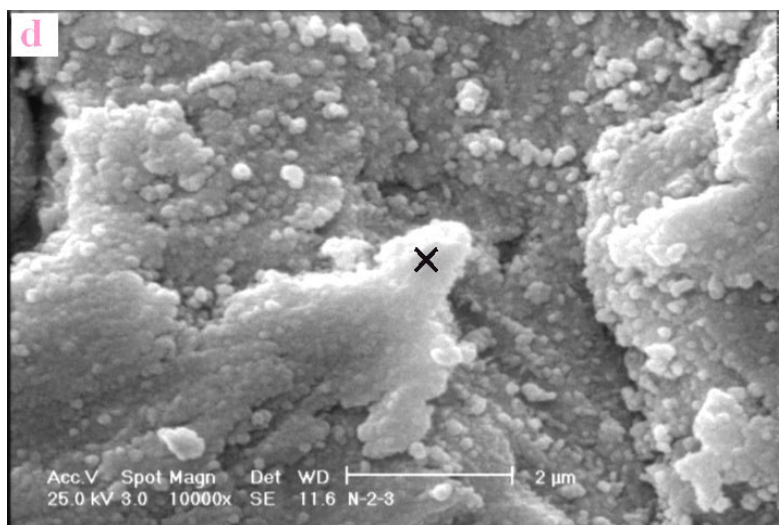


Figure 6. SEM images of cross-sectional surface area of Pb-Sb-As-S alloy with different sulfur concentration, key: (a) 0.003 wt.%, (b) 0.006 wt.%, (c) 0.009 wt.%, (d) 0.01 wt.%

Table 2. EDX elemental analysis of agglomerates on the Pb-Sb-As-S alloy surface

Wt. % Sulfur	Element	Wt. %	At. %
0.003	S K	13.17	49.49
	Sb L	0.00	0.00
	As k	0.00	0.00
	Pb L	86.83	50.51
	Total	100.00	100.00
0.006	S K	12.86	48.30
	Sb L	2.59	2.56
	As k	0.00	0.00
	Pb L	84.55	49.14
	Total	100.00	100.00
0.009	S K	13.99	50.91
	Sb L	1.62	1.55
	As k	0.00	0.00
	Pb L	84.39	47.54
	Total	100.00	100.00
0.01	S K	15.19	52.64
	Sb L	2.03	1.85
	As k	1.20	1.77
	Pb L	81.58	43.74
	Total	100.00	100.00

As can be seen, there are some agglomerates on the surfaces that their compositions were determined by using elemental analysis with SEM apparatus (Table2). The results show that the main composition of the agglomerates is lead sulfide (Pb_xS_y). As it can be observed from the figures, PbS exists as garbage in the alloy. With increasing sulfur concentration from 0.003wt% to 0.01wt% the stoichiometric ratio of lead and sulfur (x/y) decreases.

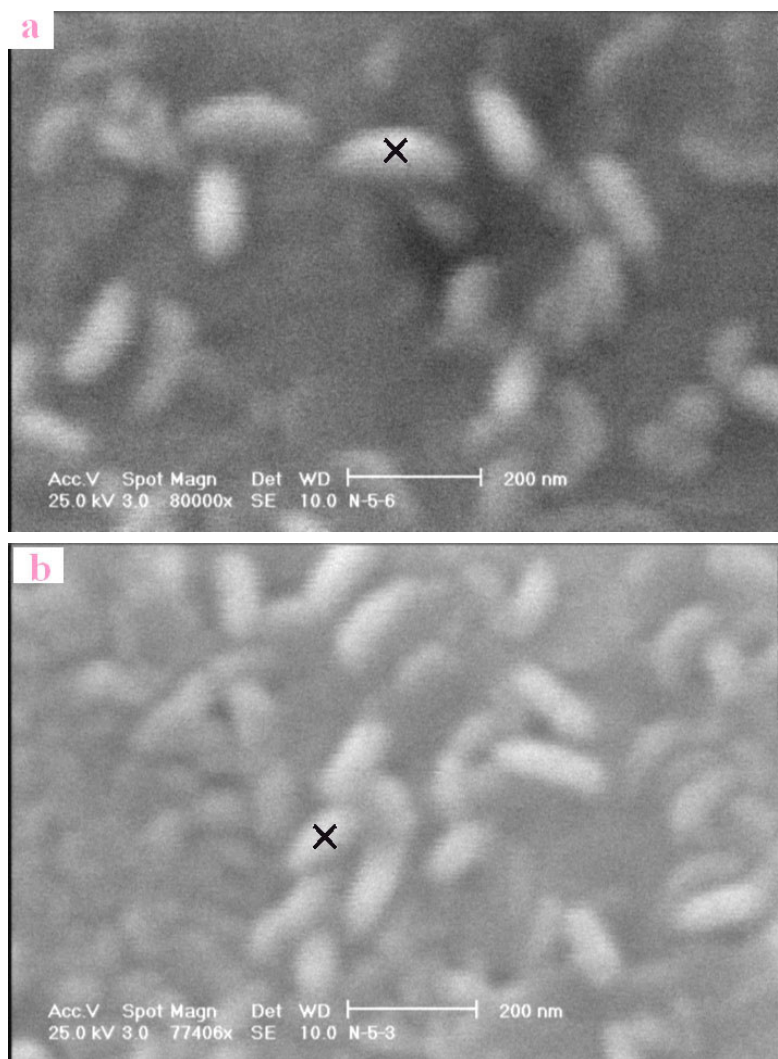


Figure 7. SEM images of $Pb_xSb_yAs_zS_w$ phase with two sulfur concentrations: (a) 0.006 wt. %, (b) 0.009 wt. %

As mentioned, PbS acts as nuclei for crystallizing lead- antimony- arsenic alloys. Fig. (7a,b) shows the scanning electron microscopy images of $Pb_xSb_yAs_zS_w$ phase. The analysis of these phases is shown in Table 3.

Comparing the data in Table2 and Table3 we can see that sulfur precipitates not only as PbS composition but also induces in the $Pb_xSb_yAs_z$ phase.

Table 3. EDX elemental analysis of the phases on the Pb-Sb-As-S alloy surface that were marked on the Fig.7a, b

Wt. % Sulfur	Element	Wt. %	At. %
0.006	S K	12.23	46.64
	Sb L	1.57	1.57
	As k	0.86	1.41
	Pb L	85.34	50.37
	Total	100.00	100.00
0.009	S K	12.88	47.69
	Sb L	2.09	2.04
	As k	1.51	2.40
	Pb L	83.52	47.87
	Total	100.00	100.00

3.4. CV

Fig.8 shows the cyclic voltammograms of Pb-Sb-As alloy for 10th, 20th, 30th, 40th cycles. In Fig.8, two anodic peaks a,b are observed in the positive sweep, and correspond to the transformation of PbSO_4 to $\beta\text{-PbO}_2$ and evolution of oxygen, respectively. A cathodic peak c in the negative sweep corresponds to the reduction of PbO_2 [16].

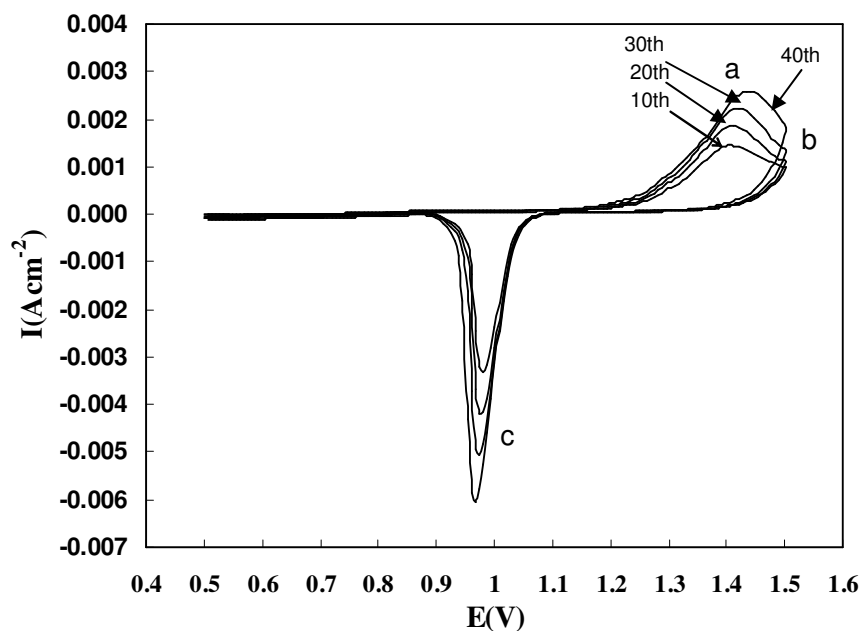


Figure 8. Cyclic voltammograms of Pb-Sb-As-S electrodes between 0.5-1.5V in 1.28 H_2SO_4 solution; sweep rate= 20mVs^{-1}

It is well known that β -PbO₂ is effective on lead-acid battery capacity. The potential region of β -PbO₂ was determined from curves that it was 1.45V. The β -PbO₂ formation is related to the peak current of i_p . It can be seen that, i_p increases proportional to cycles number. This phenomenon explains that deposited lead sulfate layers become regulated with electrochemical process.

3.5. EIS

At first, the working electrode was controlled at a constant potential of 1.45V for 60min, to produce a stable film of β -PbO₂ and then impedance measurements were performed in 1.28 sp.gr H₂SO₄ solution at 25°C in the range of 100 kHz to 1 mHz with an AC voltage signal of 10 mV. Fig. 9 shows the Nyquist plots of impedance of electrodes.

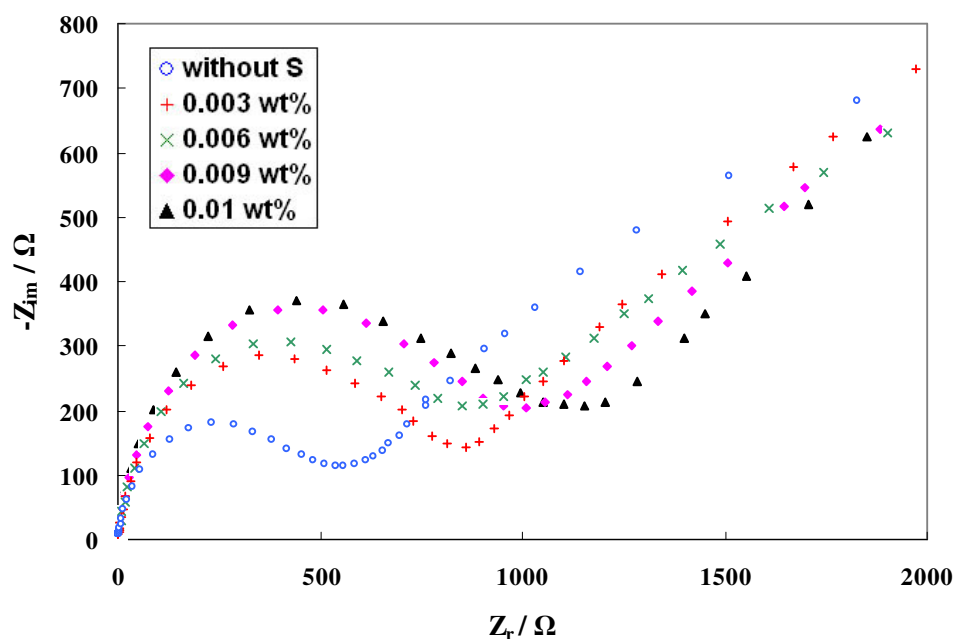


Figure 9. Nyquist plots of Pb-Sb-As-S alloy electrodes with different sulfur content at 1.45V

It can be observed that the simulated plots fit the experimental plots well. This indicates that the equivalent circuit can really reflect the electrode reaction process.

The corresponding Bode plots are presented in Fig. 10 and 11. The Nyquist plot of impedance of the electrodes shown in Fig. 9 consists of a semicircle and a straight line. The semicircle is related to charge transfer resistance and double layer capacitance. The straight line ascribes to Warburg impedance due to diffusion process. It can be observed that the diameter of semicircle that is related to charge transfer resistance increases with the addition of sulfur.

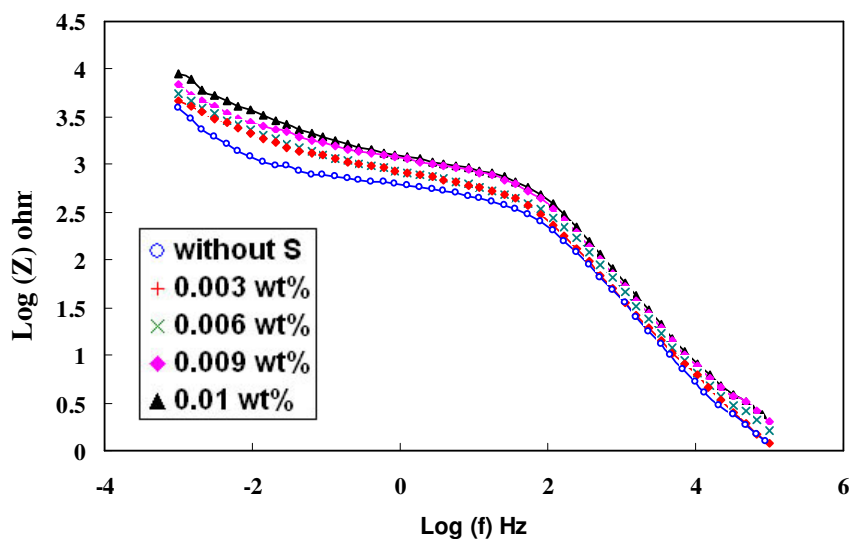


Figure 10. Bode plots of Pb-Sb-As-S alloy electrodes with different sulfur content at 1.45V. modulus against frequency

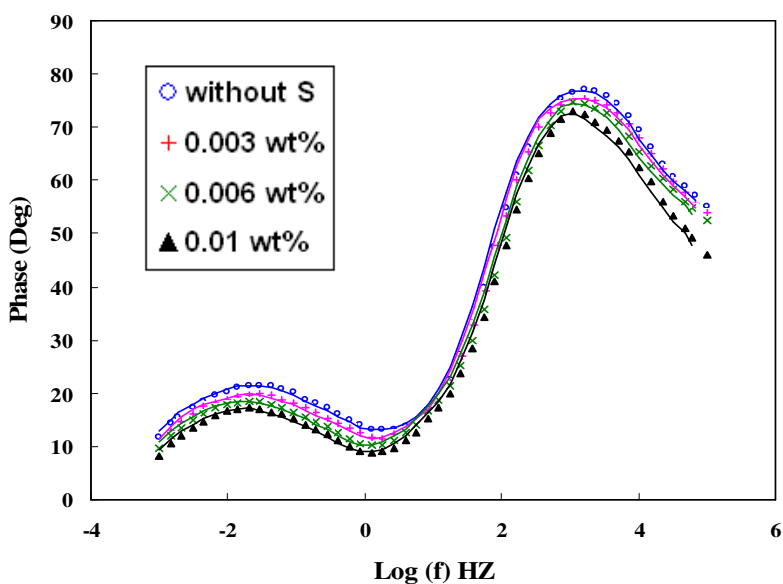


Figure 11. Bode plots of Pb-Sb-As-S alloy electrodes with different sulfur content at 1.45V. phase against frequency.

3.6. Hydrogen evolution

Hydrogen evolution reaction rate on the electrodes with different sulfur concentrations was measured by cyclic voltammetry between -0.65 and -1.85V versus Hg/Hg₂SO₄ reference electrode at a

rate of 20mVs^{-1} . The result of hydrogen evolution is shown in Fig. 12, which indicates that, with addition of sulfur the overpotential of hydrogen evolution increases and reaction rate decreases.

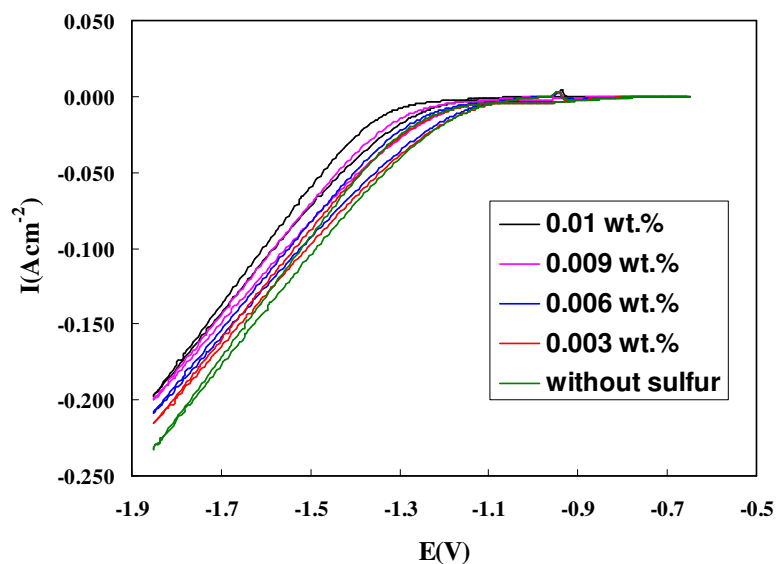


Figure 12. Hydrogen evolution reaction rate at 50th cycle on Pb-Sb-As-S alloy electrodes with different sulfur addition; sweep rate= 20mVs^{-1} in $1.28\text{H}_2\text{SO}_4$ solution $T=25^\circ\text{C}$

According to Papageorgiou and Skyllas-Kazacos's view [17], hydrogen evolution reaction was related to electrode surface morphology and microstructure. With addition of sulfur, PbS is produced. In the absence of lead sulfide nuclei, producing a columnar structure will occur on the cool walls of the mould. Columnar structure is not desired because it leads to non-uniform distribution of antimony, which contributes to increased gassing rates. So, sulfur eliminates the columnar structure, leads to uniform distribution of antimony and suppresses hydrogen evolution. Probably sulfur can affect the hydrogen-to-metal bonding energy, thus influences the hydrogen evolution reaction rate.

3.7. Oxygen evolution

When a Pb electrode is immersed in H_2SO_4 solution and polarized anodically in the PbO_2 potential region, the $\text{Pb/PbO}_2/\text{PbSO}_4/\text{H}_2\text{SO}_4/\text{H}_2\text{O}/\text{O}_2$ electrode system is established [18]. According to the potential/pH diagram [19], two redox reactions occur on the electrode: one is the oxygen evolution or reduction, and the other, the oxidation of PbSO_4 or reduction of PbO_2 . The oxygen evolution reaction occurs at the anodic layer-electrolyte interface and its rate is affected by the quantity of PbO_2 on the electrode. Cyclic voltammetry was used to this measurement. Oxygen evolution test was performed after the working electrode was hold at a constant potential of 1.45V for 60min , to produce a steady film of PbO_2 , and then was swept with 20mVs^{-1} from 1.2V to 1.5V . The result is shown in Fig.13 for

50th cycle. It indicates that the addition of sulfur slightly affects the oxygen evolution. It decreases the oxygen evolution and deduction is proportional to the sulfur content.

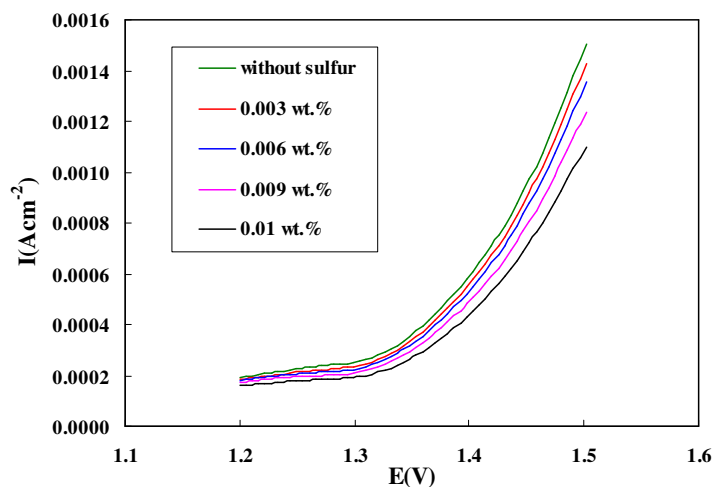


Figure 13. Oxygen evolution reaction rate at 50th cycle on Pb-Sb-As-S alloy electrodes with different sulfur additions; sweep rate= 20mVs^{-1} in $1.28\text{H}_2\text{SO}_4$ solution, $T=25^\circ\text{C}$

It is proposed that either sulfur decreases the number of active centers available for the oxygen evolution or it increases the activation energy needed for reaction to proceed. Sulfur as an alloying additive increases the overpotential of the oxygen evolution reaction on a Pb/PbO₂ electrode.

3.8. Hardness

Fig. 14 illustrates that sulfur addition increases the hardness of the alloy. The curve shows the as-cast grids hardness versus sulfur content of the alloy after one week (under atmospheric condition). Sulfur in the alloy compositions, acts as a stabilizer for the antimony and leads to a hardened lead with a finer and denser grain structure. This grain refinement characteristics brought by addition of sulfur created a lead alloy that was corrosion resistant along with greatly reduced inter-granular corrosion. When the antimony content in lead is relatively low (<2 wt.%), the influence of additives such as sulfur is more effective. Probably sulfur removes the columnar structure in the lead alloy.

3.9. Discharge capacity evaluation

The results of cycling tests of cells with 0, 0.003, 0.006, 0.009 and 0.01wt. % sulfur content in the positive grid alloy composition are presented in Fig. 15. As Fig.15 shows, the battery with sulfur content of 0.01wt.% has the highest discharge capacity. The use of sulfur with weight percent of 0.01wt. % causes (48.67%) increase in the first discharge capacity of positive plates. The time of reaching to cut off voltage of 1.5V was used as a parameter for comparison of the batteries.

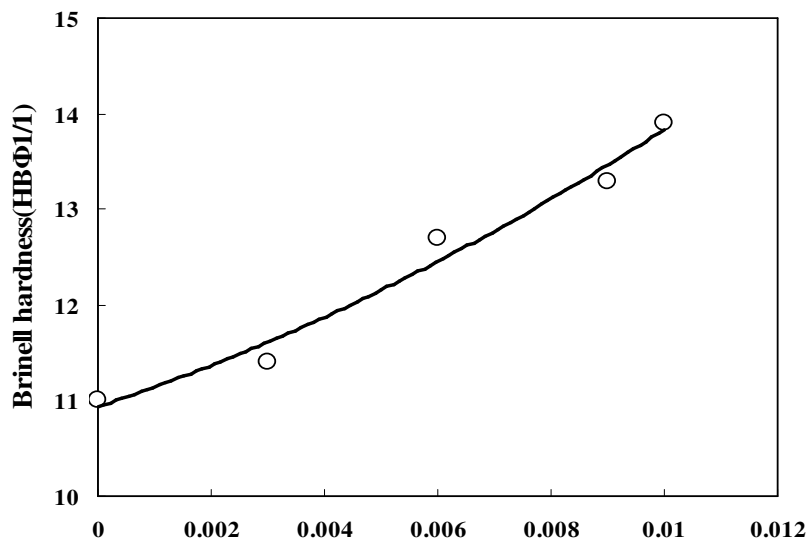


Figure 14. Hardness of Pb-Sb-As-S alloys after one week

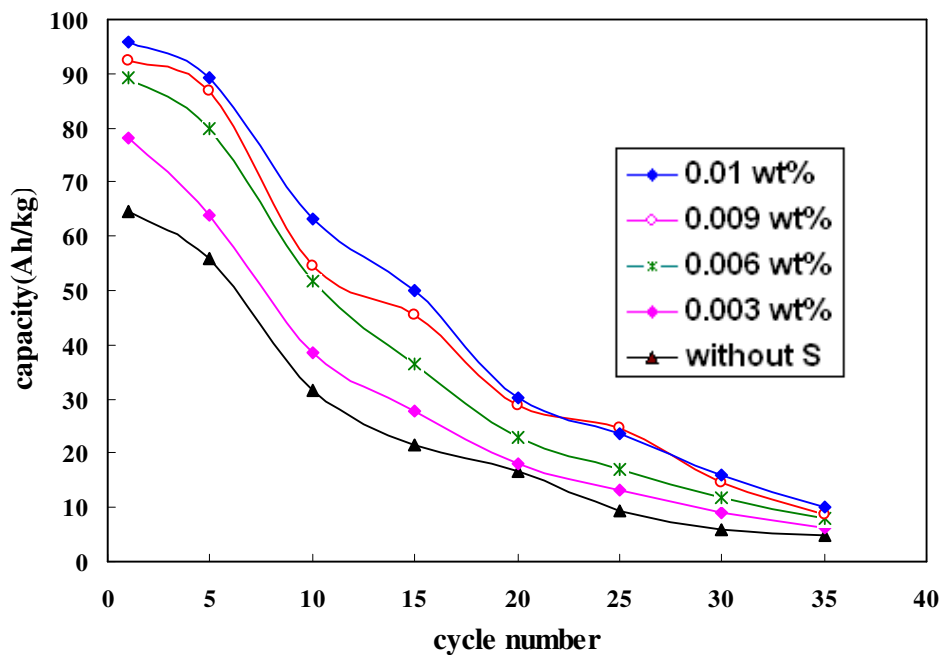


Figure 15. Discharge capacities for the different percentages of sulfur as a positive grid additive at discharge current of 1A

The battery with 0.01wt. % sulfur content has the highest discharge capacity that it can probably be related to a good corrosion resistance of the alloy. Corrosion layer plays a key role in the life cycle of the battery as it helps to adhesion of the grid and active material but, the exceedingly corrosion layer

thickness, causes an decrease in its conductivity and also reduces the adhesion of the paste to the grids and the paste starts shedding.. These results showed that the discharge capacity of the positive grids with 0.01wt. % sulfur content in 30th cycle is (167.80%) more than positive grids without sulfur.

As mentioned in the previous sections, sulfur addition increases corrosion resistance of the alloys.

3.10. CA

Chronoamperometry is a potential step technique in which the potential of the working electrode is changed instantaneously from initial to final value and the current-time response is recorded. A certain potential-time (Fig. 16) profile is applied to the working electrode.

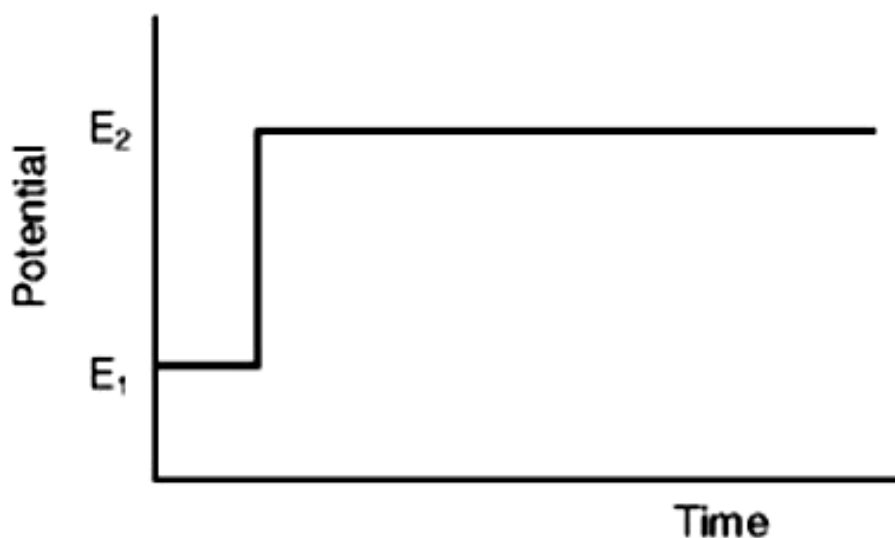


Figure 16. Potential- time profile

E_1 should be a potential at which neither reduction of analyte species nor any electrode reactions occur. At zero time, the potential is instantaneously changed to a new value, E_2 , at which the reduction of electrolyte species occurs at diffusion controlled rate. The current will decrease with time because current is a function of the concentrations of electrolyte species at the electrode surface. For a diffusion-controlled current, the current-time (i - t) curve is described by the Cottrell equation:

$$i = nFACD^{1/2} \Pi^{-1/2} t^{-1/2}$$

where n is the number of transferred electrons, F : Faraday's constant (96500 Cmol^{-1}), A : electrode surface area (cm^2), D : diffusion coefficient (cm^2s^{-1}) and C : concentration (molcm^{-3}). The charge-time (Q - t) (the Anson equation) is obtained by integrating the Cottrell equation:

$$Q = 2nFACD^{1/2} \Pi^{-1/2} t^{1/2}$$

In order to investigate the formation of β -PbO₂, a very convenient experimental method is the one based on the analysis of CA. Fig.17 shows the CA curves for the alloys with and without sulfur in the β -PbO₂ potential region (1.45V).

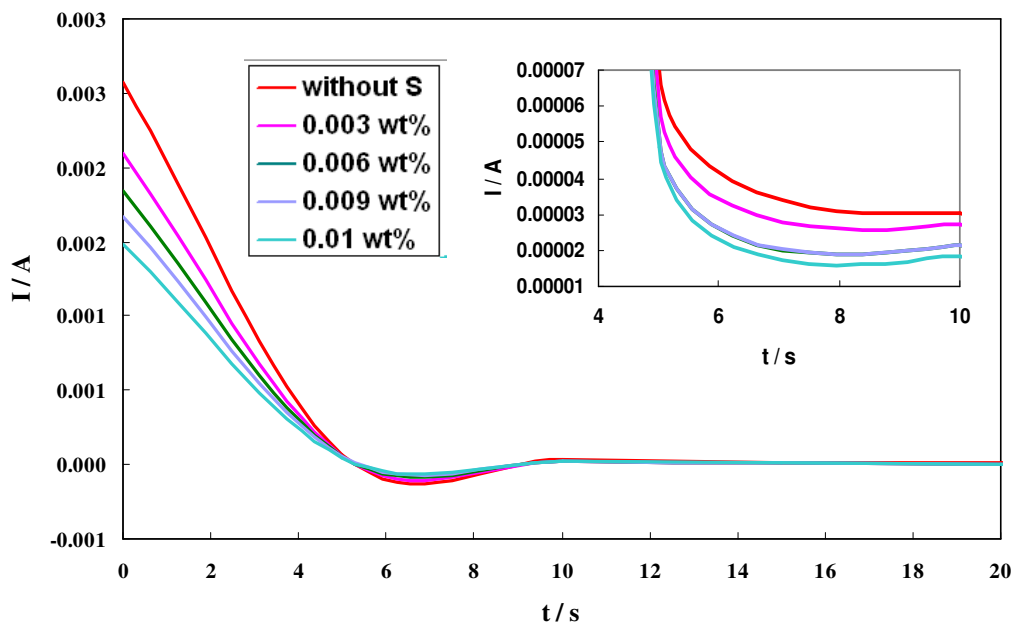


Figure 17. Current –time responses during β -PbO₂ film formation at 1.45V on Pb-Sb-As-S alloy electrodes with different sulfur addition

From the CA curves, it is possible to determine the value of Q by integration of an area in the current transient (Fig.18) that is directly proportional to the value of produced β -PbO₂ on the alloy surface.

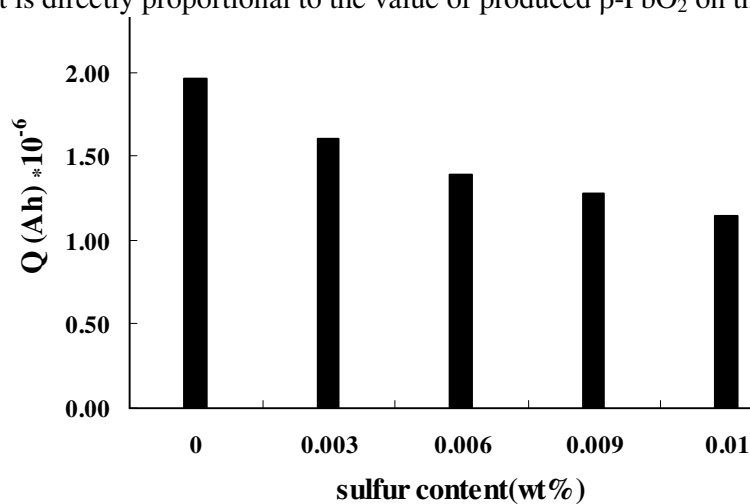


Figure 18. Charge–time responses during β -PbO₂ film formation at 1.45V on Pb-Sb-As-S alloy electrodes with different sulfur additions

Fig.18 shows that, sulfur added to lead alloy can more effectively inhibit the growth of the anodic β -PbO₂ film. The anodic β -PbO₂ stable film grown on the lead alloy avoids the current to flow to the grids [20].

4. CONCLUSIONS

- Generally with increasing sulfur concentration, the corrosion current density and corrosion rate decrease and polarization resistance increases.
- Both hydrogen and oxygen evolution on Pb-Sb-As alloys are decreased by sulfur addition.
- The sulfur addition in the studied composition range causes an improvement in positive grid hardness.
- Discharge capacities of positive grids with different sulfur content are more than positive grids without sulfur.
- SEM examinations show that with increasing sulfur content, the stoichiometric ratio of lead and sulfur(x/y) decreases and PbS exists as garbage in the lead alloys.
- Sulfur is less toxic than other alloying additives. Sulfur dose not increase the contamination by dross and dose not quickly burn out of the molten material when it has been completely incorporated in the alloy.

ACKNOWLEDGEMENTS

The authors gratefully acknowledge the financial supports from Niru Battery Manufacturing Company.

References

1. Kenneth Peters, US Patent 3912537 (Oct. 14, 1975).
2. S. Nijhawan, US Patent 3801310(April 2, 1974).
3. N.E. Bagshaw, *J. Power Sources* 53 (1995) 25
4. Ranna K. Hebbbar, US Patent 4158563 (Jun. 19, 1979).
5. D. Pavlov, M. Dimitrov, G. Petcova, *J. Electrochem. Soc.* 142 (9) (1995) 2919
6. Cui Ronglong and Wu Shousong, *J. Power Sources*, 46 (1993) 327
7. L.T. lam, T.D. Huynh, N.P. Haigh, J.D. Douglas, D.A.J. Rand, C.S. Lakshmi, P.A. Hollingsworth, J.B. See, J. Manders, D.M. Rice, *J. Power Sources* 53 (1995) 63.
8. D.A.J. Rand, D.P. Boden, C.S. Lakshni, R.F. Nelson, R.D. Prengaman, *J. Power Sources* 107 (2002) 28.
9. R.D. Prengaman, US Patent 6649306 B₂ (2000).
10. R.D. Prengaman, *J. Power Sources* 95 (2001)224.
11. P. Rao, US Patent 5298350 (1994).
12. P. Rao, T.F. Uhlemann, US Patent 5691087 (1997).
13. Armin Ueberschaer, US Patent 3993480 (Nov. 23, 1976).
14. Bockris J O M, Reddy A K N, *Modern electrochemistry [M]*. New York: Plenum, 1970, pp. 889.
15. J.C. Lin, R.C. Sharma, and Y.A. Chang, *Bull. Alloy Phase Diagrams*, 7 (4) (1986) 374

16. W.-F. Zhou, H.-T. Liu, C. Wei, J. Sun, *Acta Chimi. Sin.* 44 (1986) 399.
17. N. Papageorgiou, M. Skyllas-Kazacos, *Electrochim. Acta* 37 (1992) 269
18. D. Pavlov, 'Power Sources for Electric Vehicles', (Edited by B.D. McNicol and D.A.J. Rand), Elsevier, Amsterdam (1984) pp.167.
19. P. Ruetschi, *J. Electrochem. Soc.* 120 (1973) 331.
20. F.E. Varela, E.N. Codaro, J.R. Vilche, *Journal of Applied Electrochemistry* 27 (1997) 1232